Springer

KSME

Journal of Mechanical Science and Technology 30 (11) (2016) 4833~4843
www.springerlink.com/content/1738-494x(Print)/1976-3824(Online)
DOI 10.1007/s12206-016-1002-z

A modified adaptive filtering algorithm with online secondary path identification used for suppressing gearbox vibration †

Weijin Gao*, Liang Wang and Yongguang Liu

School of Automation Science and Electrical Engineering, Beihang University, Beijing, 100191, China

(Manuscript Received October 12, 2015; Revised May 9, 2016; Accepted June 17, 2016)

Abstract

We determined the actuator location based on the dynamic modal of gear shaft, and analyzed the feasibility of a modified filtered-x least mean square algorithm with online secondary path identification. The proposed adaptive controller is designed to drive the actuators for preventing the vibration caused by gear backlash from a gear pair passing to the external gear housing structure. For the vital identification system, a changed identification input with error energy is presented to reduce the impact of additive random noise on the whole system. To ensure a realistic assessment of the proposed control strategy, numerical studies were implemented for a gearbox used by NASA-GRC. The simulation results validate the efficiency of the proposed approach through promising vibration control results that will guide future experimental work.

Keywords: Gearbox vibration; Modified Fx-LMS; Online identification; Error energy

1. Introduction

Gearbox systems, as a crucial power-outputting mechanism, are widely used in various of fields such as shipping, aviation, wind power and automotive industry. As well known, whether in defence or civil field, a large amount of equipment is being designed with such characteristics as light-weight, large-scale and high-speed. Under these circumstances, the vibration and noise produced by gear pair assembly would be amplified or attenuated through equipment components. For gearboxes, gears are critical elements that produce vibration because of factors like backlash and time-varying stiffness. In very serious cases, gear vibrations maybe reduce the life and performance of the transmitting components [1]. Although the gearbox vibration generation phenomenon is quite complex due to its assembly relations, periodic characteristics of the gearbox vibration signal make the problem a likely candidate for solving by applying active control, and some researches validated the efficiencies of this control strategy [2-5].

Since vibration is widely regarded as an evaluation of the total quality of machines, its reduction is highly desired. Such methods as active vibration control and dynamic optimization should be taken especially by virtue of intelligent material actuators and computers. Montague applied a manually controlled analog phase shifter with an amplifier to drive a set of piezoelectric actuators attached to the shafts supporting the gear pair [6]. Thus, vibration was reduced to 70 % or so at the fundamental gear mesh frequency presented in their experiments. However, the method proposed by Montague had a shortcoming in that the manual tuning process was inefficient since it had to be adjusted separately under different operating speeds. After that, Rebbechi et al. [7] proposed a more automated active control strategy with a popular adaptive feedforward controller. They employed a pair of magnetostrictive actuators mounted at the bearing locations to prevent the vibration transmission from the shaft and gear housing. Unlike the study by Montague et al., the vibration response of the first three harmonics was suppressed that an attenuation of 20-28 dB at the fundamental mesh frequency, and that reduction of less than 10 dB at the second and third mesh harmonics. Subsequently, a new concept was realized by Brennan and Chen [8] where three magnetostrictive actuators were directly mounted onto the side of one of the gear pairs to suppress the torsional vibrations due to the circumferential forces generated by the actuators. They utilized a frequency domain adaptive harmonic controller designed for nonlinear systems, and the results yielded about 7 dB of reduction in gear angular vibrations at the mesh frequencies. In addition, Lim et al. [9, 10] adopted a similar concept used by Brennan to deal with the gear pair torsional and translational vibrations simultaneously using a new direct hybrid adaptive controller. However, there exists the major drawback for this actuation concept since it requires complex slip rings to transfer electric power to the

*Corresponding author. Tel.: +86 13001203677, Fax.: +86 1082316423
E-mail address: wangliang@buaa.edu.cn
† Recommended by Associate Editor Cheolung Cheong

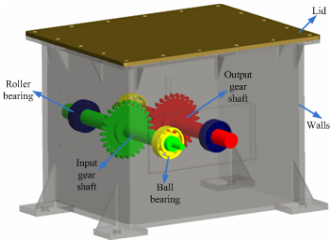

Fig. 1. Three dimension model of gearbox.

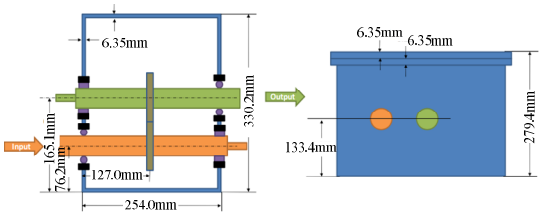

Fig. 2. A schematic of the gearbox with key dimensions.

actuators. Something worth paying attention to is that Guan et al. [11] compared the performance of different actuation concepts proposed before, and pointed to the actuation concept that active shaft transverse vibration control as the most feasible control strategy. In particular, Guan, Lim and their coworkers have done much research work by the usage of this feasible approach [12]. In their studies, they used an enhanced Fx-LMS (Filtered-x least mean square) algorithm, and also employed an additive random noise technology to identify the secondary path characteristics in online or offline mode. Ultimately, their numerical study results validated the efficiency of the proposed control concept.

By the way, we studied gearbox vibration suppression by using the active shaft transverse vibration control with considering the backlash and the stiffness between gear teeth treated as average stiffness. As is well known, for a closed-loop control system, the position actuator placement is of importance to the system performance; even in a severe case, the bad actuator placement would lead to the control spillover. In the studies presented above, the actuation position is located at one-third of the length from the gear position to the bearing support location. While in this work the actuator is placed by considering the shaft natural modes that affect the dynamic performance of itself. In addition, a modified Fx-LMS algorithm with online identification is studied. To ensure that the simulations are sufficiently realistic, the practical design parameters are used in computations. The numerical simulation and analysis is intended to be a precursor to future experimental work.

2. Vibration description of gearbox

We used a gearbox (NASA-GRC) [13] as the object investigated, which consists of gears, shaft, bearings and gear housing, seen in Fig. 1. In addition, more details for the gearbox can be found in Refs. [14-16], and a schematic of the gearbox with key dimensions is shown in Fig. 2. Parameters of gear are given in Table 1.

Table 1. Parameters of gear.

Number of tooth	28
Tooth width (mm)	6.35
Tooth thickness (mm)	4.851
Pressure angle (°)	20
Modulus	3.175
Center distance (mm)	88.9
Tip diameter (mm)	95.25
Root diameter (mm)	79.73

Table 2. Parameters of bearings.

Parameters	Roller bearing	Ball bearing
Number of rows	1	1
Number of rolling elements	13	9
Contact angle (°)	0	0
Pitch diameter (mm)	39.00	38.50
Roller length (mm)	8.60	7.90
Roller diameter (mm)	7.50	7.90
Bearing width (mm)	15.00	15.00
Outer diameter (mm)	52.00	52.00
Outer diameter of inner raceway (mm)	31.50	34.40
Inner diameter of outer raceway (mm)	46.40	46.30

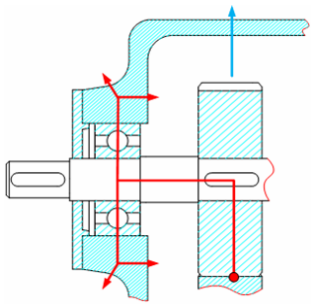

Fig. 3. Schematic diagram of vibration transmission.

For this gearbox, such nonlinear factors as gear backlash and time-varying mesh stiffness were considered in the dynamic model [17, 18]. Just due to these factors, vibration would be produced when gears meshed in different operating conditions. Thus the vibration will be propagated from gears to gear housing based on the assembly relationship. Especially bearings, as transition pieces, should be selected rationally. Relative parameters of bearings selected in this study are shown in Table 2. Fig. 3 shows energy flows through the gear unit assembly. So, to get better control of the vibration, an active control strategy needed to be designed, and that was the purpose of this study.

2.1 Force model of gear-meshing

The equivalent model of a pair of meshing teeth is shown in

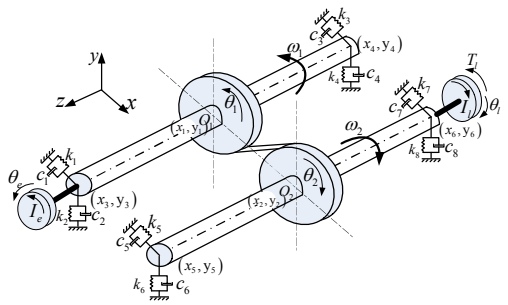

Fig. 4. Dynamic model of gear transmission system.

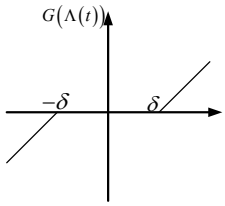

Fig. 5. Gear backlash function.

Fig. 4. $(O_1x_1y_1)$ and $(O_2x_2y_2)$ are the fixed reference frames of driving gear and driven gear, respectively. ω_1 and ω_2 are the angular velocity of input shaft and output shaft, respectively.

According to the gear pair model shown in Fig. 4, the relative displacement along the line of action of the gear mesh is expressed as follows:

$$\Lambda(t) = \theta_1 r_1 - \theta_2 r_2 + (x_1 - x_2)\sin\alpha + (y_1 - y_2)\cos\alpha - e \tag{1}$$

where θ_1 and θ_2 are the torsional angle displacement of driving gear and driven gear, respectively. α is the meshing angle, the value of which is equal to the pressure angle; e is the gear mesh error; r_1 and r_2 represent the base radius of the input gear and output gear, respectively; and x_1, x_2, y_1, y_2 denote the vibration displacements in the reference frames.

In this paper, gear backlash is considered and shown in Fig. 5. Provided that gear backlash is 2δ and gear backlash function can be written as

$$G(\Lambda(t)) = \begin{cases} \Lambda(t) - \delta & \Lambda(t) > \delta \\ 0 & -\delta \le \Lambda(t) \le \delta \\ \Lambda(t) + \delta & \Lambda(t) < \delta. \end{cases} \tag{2}$$

According to Eqs. (1) and (2), the dynamic force of gear meshing can be given by

$$F(t) = k \cdot G(\Lambda(t)) + c \cdot \dot{\Lambda}(t), \tag{3}$$

where k is the mesh stiffness and c is the mesh damping.

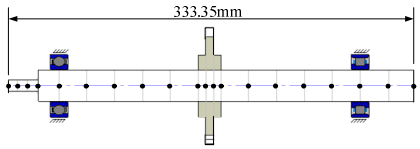

Fig. 6. Schematic diagram of gear shaft with nodes.

For the geared-rotor system shown in Fig. 1, provided that gears, shafts and bearings are linear elastic bodies. In the static condition, components of the system are installed at the exact location in theory. Fig. 4 shows the dynamic model of gear transmission system.

3. Configuration of actuator location and interaction model between actuator and shaft

3.1 Configuration of actuator location

In the process of active vibration control, it is obvious that the position of actuators determines the control performance of system. In this study, two actuators are placed onto the gear shaft with considering the symmetry of gear shaft, which produce active control force to the shaft according to signals from accelerometers mounted onto the shaft. The two actuators here play two roles: To reduce the meshing forces and to prevent the vibration generated by gear meshing from propagating to gear housing. To get the appropriate placement, actuators are placed in terms of gear shaft mode shapes. A schematic diagram of the gear shaft with nodes is shown in Fig. 6.

For the elastic gear shaft shown in Fig. 6, the dynamic equation of finite element is given as follows:

$$M_s\ddot{u} + C_s\dot{u} + K_s u = F_m, \tag{4}$$

where M_s, K_s and C_s are the generalized mass, stiffness and damping matrix, respectively; u is the displacement vector of nodes; and F_m is the external force vector. To get the vibration mode shapes of gear shaft, make $C_s = 0$ and $F_m = 0$, and Eq. (4) can be written as:

$$M_s\ddot{u} + K_s u = \mathbf{0}. \tag{5}$$

In terms of Eq. (5), let $u = \tilde{u}\sin(\omega t + \psi)$, for a N degree-of-freedom elastic gear shaft, its eigen pairs are $(\omega_1^2, \tilde{u}_1)$, $(\omega_2^2, \tilde{u}_2), \cdots, (\omega_N^2, \tilde{u}_N)$. For convenience, the eigenvectors are normalized as follows:

$$\phi_n = \begin{bmatrix} \phi_{1n} \\ \phi_{2n} \\ \vdots \\ \phi_{Nn} \end{bmatrix} = \frac{1}{(\tilde{u}_{jn})_{\max}} \begin{bmatrix} \tilde{u}_{1n} \\ \tilde{u}_{2n} \\ \vdots \\ \tilde{u}_{Nn} \end{bmatrix} \quad (j = 1, 2, \cdots N). \tag{6}$$

The vibration mode shape matrix can be given:

Table 3. The first six natural frequencies of gear shaft.

Orders	Frequency (Hz)
1	602.01
2	2916.8
3	4461.6
4	6561.9
5	8601.4
6	12222.4

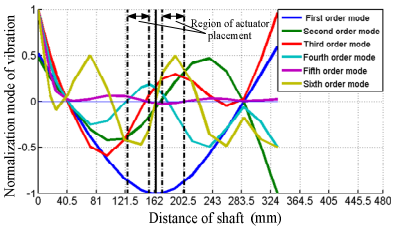

Fig. 7. Region of actuator placement.

$$\phi = \begin{bmatrix} \phi_1 & \phi_2 & \cdots & \phi_N \end{bmatrix} = \begin{bmatrix} \phi_{11} & \phi_{12} & \cdots & \phi_{1N} \\ \phi_{21} & \phi_{22} & \cdots & \phi_{2N} \\ \cdots & \cdots & \cdots & \cdots \\ \phi_{N1} & \phi_{N2} & \cdots & \phi_{NN} \end{bmatrix}, \quad (7)$$

where ϕ is the mode shape matrix.

On the basis of Eq. (5), the first six natural frequencies of the gear shaft are given in Table 3. As the mesh force is considered for the vibration source with gear backlash $\delta = 0.1778$ mm, mesh frequency should be given according to the formula $f_{mesh} = Z * RPM / 60$, where RPM is the speed of revolution. Here, considering that the operating conditions are in the range of 1000~5000 RPM, the maximum mesh frequency is 2333.3 Hz. Hereby compared with the natural frequencies of gear shaft, the first two natural frequencies should be emphasized under the operating conditions.

For the better description of dynamic characteristics of gear shaft, the first six natural frequencies are taken into account. Thereby, based on the mode shapes of gear shaft, the region of actuator placement is described in Fig. 7, where actuators are not placed onto the nodal line (dimensionless displacement is zero). Obviously, if an actuator is placed onto the nodal line, there will be no control action and even the entire system becomes unstable.

According to Fig. 7 and node position of gear shaft, two actuators are symmetrically attached to the driven shaft at the position of 143.596 mm away from the shaft end using an additional set of bearing as illustrated in Fig. 8. The actuators are acting against the redundant bearings along the line-of-action of mesh force of gear pair. Notably, although the dynamic force is still being transmitted between the shaft and gear housing, the added bearings do not carry the required static load. Therefore, these two bearings can allow a large range of motion. Moreover, due to the possible run-out and vibration deformation of the gear shaft, some lateral motions may be harmful to the actuators. Hence, the setup should be specially designed such that the actuators are not directly connected to the bearing raceway in real engineering. In some researches, a good suggestion is that a stinger rod links the bearing raceway and the actuator, thereby the potentially harmful lateral forces in the actuators are reduced in virtue of providing some degree of lateral flexibility by the stinger rod.

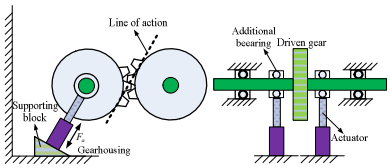

Fig. 8. Layout of actuator.

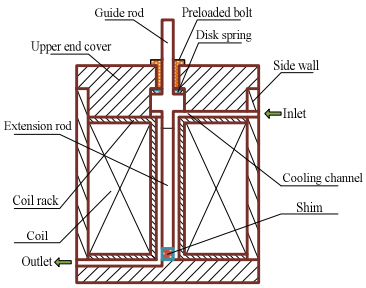

Fig. 9. GMA model.

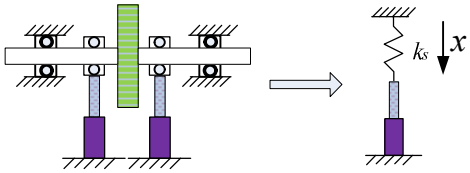

Fig. 10. Interaction model between actuator and shaft.

3.2 Interaction model between actuator and shaft

Assuming that the gear system is linear and the gear backlash will not change after the actuator is installed in real engineering, it is relatively easy to determine the required active force for efficiently suppressing the gear housing vibration by the actuator. A Giant magnetostrictive actuator (GMA) is used in this paper as shown in Fig. 9.

For the actuator, theoretically, the output force can be expressed by

$$F = NI / \left(R_m d_{33} \right), \quad (8)$$

where N is coil turns, I is coil current, R_m is of magnetic reluctance, and d_{33} is piezomagnetic strain constant.

When the actuator is applied on a shaft structure, the simplified interaction model between actuator and shaft is shown in Fig. 10, where an equivalent spring load is utilized and its

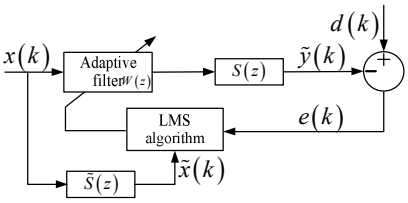

Fig. 11. A block diagram of Fx-LMS algorithm.

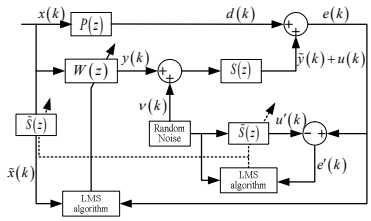

Fig. 12. Fx-LMS algorithm with online identification.

stiffness is k_S.

According to active vibration control principle, an active actuation equation can be given by

$$k_A(x_a - x) - k_S x = 0, \tag{9}$$

where x_a is the stroke of the actuator; k_A is the equivalent magnetostrictive stiffness calculated from experimental results or a finite element modeling. In addition, the effective force applied on the shaft depends on the stiffness of the shaft and the effective magnetostrictive stiffness. The stiffer the shaft is, the more force the actuator can generate.

4. Multichannel adaptive filtering algorithm

4.1 Standard Fx-LMS algorithm

In practical applications, the Fx-LMS algorithm is widely used with its advantages such as easy hardware implementation and great robustness. A popular block diagram of Fx-LMS algorithm is described in Fig. 11, which normally consists of a reference sensor, a control unit and an actuator.

For the block diagram of Fx-LMS algorithm given in Fig. 11, the error signal $e(k)$ is expressed as:

$$e(k) = d(k) - \tilde{y}(k). \tag{10}$$

According to Fig. 11, Eq. (10) can also be written as:

$$e(k) = d(k) - S(z) * \left[x(k) * W^T(k)\right], \tag{11}$$

where $S(z)$ is the secondary path, $W(k)$ is the coefficient vector of $W(z)$ at time k and $x(k)$ is the reference signal vector at time k.

The objective of the adaptive filter is to minimize the instantaneous square error $e^2(k)$:

$$\min J = \min E\left\{\left|e(k)\right|^2\right\}. \tag{12}$$

And the coefficients are updated by using the LMS (Least mean square) algorithm, then the weight updating equation can be written as:

$$W(k+1) = W(k) + 2\mu e(k)\tilde{x}(k), \tag{13}$$

where μ is the convergence factor. Especially, $\tilde{S}(z)$ follows the adaptive filter and it must also be placed in the weight updating path, namely, the name Fx-LMS.

$$\tilde{x}(k) = \tilde{S}(z) * x(k), \tag{14}$$

where $\tilde{S}(z)$ is the estimated impulse response of the secondary path filter $S(z)$.

4.2 Modified Fx-LMS algorithm

For a secondary path with time-varying characteristics, especially of gearbox system, the online modeling technique is more suitable [3]. In Lim et al., a similar identification technique for secondary path to the method proposed by Eriksson [19]. Fx-LMS algorithm with online identification is seen in Fig. 12.

From the data flow in Fig. 12, the weights $\tilde{S}(z)$ are updated by the LMS (Least mean square) algorithm in the following form:

$$\begin{aligned}\tilde{S}(k+1) &= \tilde{S}(k) + \mu_v v(k) e'(k) \\ &= \tilde{S}(k) + \mu_v v(k)\left[e(k) - u'(k)\right] \\ &= \tilde{S}(k) + \mu_v v(k)\left[v(k) * S(k) - v(k) * \tilde{S}(k)\right] + \mu_v v(k)\Theta(k)\end{aligned} \tag{15}$$

where $\Theta(k) = d(k) + y(k) * S(k)$. From Eq. (10), we can know that the second term of the right side is a disturbance when $\tilde{S}(k)$ converges to $S(k)$. To ensure that convergence performance, the second term must be eliminated. The identified secondary path $\tilde{S}(k)$ is also used as the compensating for the effect of the secondary path dynamics. Therefore, the equation of weights ($W(z)$) updating is given by

$$\begin{aligned}W(k+1) &= W(k) + \mu_w \tilde{x}(k) e(k) \\ &= W(k) + \mu_w \tilde{x}(k)\left[d(k) + y(k) * S(k) + u(k)\right] \\ &= W(k) + \mu_w \tilde{x}(k)\left[d(k) + y(k) * S(k) + v(k) * S(k)\right].\end{aligned} \tag{16}$$

Obviously, the term $\mu_w \tilde{x}(k) u(k)$ in Eq. (16) is in proportion to $v(k)$ and is related to $S(k)$. Thus the updating of weights $W(z)$ also suffers from a disturbance, namely, the

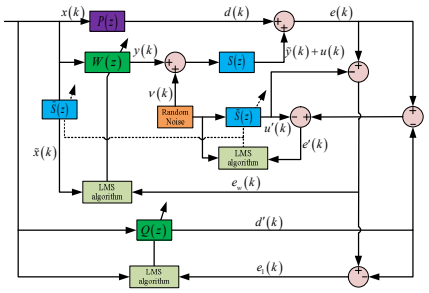

Fig. 13. Modified Fx-LMS algorithm with online identification.

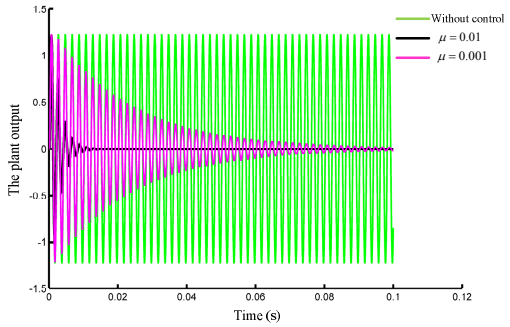

Fig. 14. The control effect with different convergence factors.

identification process has an influence on the active control path. In view of this problem, a modified algorithm is designed as follows in Fig. 13, the purpose of which is to cancel the interference between random noise and active control path.

According to Fig. 13, $e(k)$ is replaced with $e_w(k)$, which is used to adjust the weights $W(z)$. In fact, when $\tilde{S}(k) \approx S(k)$, we know that $e_w(k)$ can be written as

$$\begin{aligned} e_w(k) &= e(k) - v(k) * \tilde{S}(k) \\ &= d(k) + y(k) * S(k) + v(k) * S(k) - v(k) * \tilde{S}(k) \\ &= d(k) + y(k) * S(k) \end{aligned} \quad (17)$$

so it is said that the error signal $e_w(k)$ has no relation with $v(k)$. Furthermore, the error signal can be utilized to adjust weights $W(z)$ and be treated as the anticipation error to adjust weights $Q(z)$. Hence, this modified algorithm can solve the problem when identification of the secondary path with random noise involved.

4.3 Performance analysis of modified algorithm

In this section, some cases are selected to study the performance of proposed algorithm. For a control system based on Fx-LMS algorithm with online identification, which consists of the primary path $P(z)$, the secondary path $S(z)$, the reference signal $x(k)$, and the random noise $v(k)$, $P(z)$ and $S(z)$ are chosen as [20]

$$\begin{aligned} P(z) &= 0.001 + 0.005z^{-1} - 0.005z^{-2} + 0.75z^{-3} \\ &\quad + 0.5z^{-4} - 0.35z^{-5} - 0.4z^{-6} + 0.2z^{-7} + 0.4z^{-8} - 0.1z^{-9} \\ S(z) &= 0.01 + 0.01z^{-1} + 0.9z^{-2} - 0.01z^{-3} - 0.75z^{-4}. \end{aligned} \quad (18)$$

As we know, periodic signals appear in a variety of applications, particularly in rotating mechanical systems. So the reference signal is selected as a sinusoidal function with magnitude $A = 1$, frequency $f = 500$ Hz, and initial phase $\phi = 0$. That is, $x(t) = A\sin(2\pi ft + \phi) = \sin(1000\pi t)$. According to the Nyquist sampling theorem $f_s > 2f_{\max}$, here the sampling time is $T = 0.0001$ s determined to computational ability. Theoretically, the more information of original signal is shown, the smaller value of the sampling time is chosen.

As an addition to the system, a small amount of random noise is injected through the actuator. Since the energy introduced by random noise is required to an appropriate value, the identification input is addressed in this study by

$$v'(k) = v(k) \bullet |e_w(k)|^2, \quad (19)$$

where $e_w(k)$ is seen in Fig. 13. From Eq. (19), input is changed with the error energy, and we know that it is not identical energy in the process of identification injected into the system. Thus the random noise has less impact on the system. In our studies, $v(k)$ is white noise with zero mean and variance $\sigma = 0.001$. In addition, for the sampling time T_v of identification input, it should be satisfied with $T_v \le T$; if not, the control system will be instable. Here, we let $T_v = 0.0001$ s.

As the following, the performance of our modified Fx-LMS with online identification algorithm is examined via simulation. We will compare our algorithm with other algorithms for the same parameter settings. All simulations have been performed in Matlab/Simulink with the solver ODE45 in variable-step. Besides, the convergence factor μ can be given by [21]

$$0 < \mu < \mu_{\max} \approx \frac{2}{P_{x'}L}, \quad (20)$$

where $P_{x'}$ is the power spectrum of the filtered reference signal and L is the order of the filter. L_w, L_s, L_q are the orders of $W(z)$, $\tilde{S}(z)$, $Q(z)$, respectively. And $L_w = L_s = L_q = 32$.

For the active control system with Fx-LMS algorithm, the convergence factor μ has an important impact on the control effect. Fig. 14 shows the simulation results under the cases of different convergence factors without adding the identification.

From Fig. 14, the control effect starts to change badly when $\mu = 0.001$. In fact, the algorithm does not work when

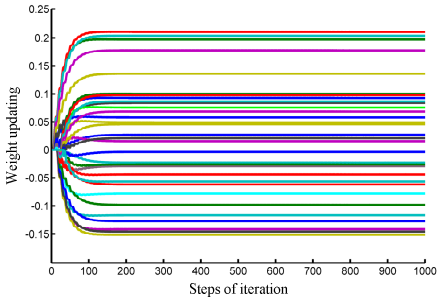

Fig. 15. The convergence performance of weights.

$\mu = 0.1$ or $\mu = 0.0001$, and the simulation results are not given in this paper. So the convergence factor is also selected as $\mu = 0.01$ in the following simulation, and in this condition, the convergence performance of weights $W(z)$ is shown in Fig. 16. Furthermore, it is concluded that μ is critical for the stability of the modified Fx-LMS algorithm. If the convergence factor exceeds the allowable limitation, as noted in Refs. [22, 23], an instability may occur. Then this limitation is approximately given by Eq. (20).

While the control system with secondary path identification, as an experimental description in Ref. [3], even though fairly good reduction was achieved for the gear housing response at the mesh harmonics, a small amount of additive noise remained in the residual signal due to the random noise as the input of secondary path identification. Fig. 16 demonstrates the active control results utilizing the proposed online identification in this paper and the previous method in Ref. [3].

In Fig. 16, the proposed method in this paper has more effective control even though the variance increases. We can note that the previous method almost has no effect on active control when $\sigma = 0.1$. From this simulation, the peak-to-peak amplitude of the plant output decreases monotonically only after 0.002 s or so in Fig. 16(a), and after 0.01s the plant output tends to a stable value that is near 0. As a fact, these phenomena can be explained by Fig. 17. The frequency response of the online identified secondary path by using the proposed algorithm is shown in Fig. 17, where the upper plot is the amplitude and the bottom plot is the phase response of the filter $\tilde{S}(z)$ with respect to normalized frequency.

Here in Fig. 17, the black solid curve represents the real response of the secondary path. The green, red curves are online identification model responses at 0.002 s and 0.01 s, respectively. As described above, we know that the frequency of external input is 500 Hz. From the phase response in Fig. 17, the phase of the identified filter at 0.002 s is approximately $-\pi/2$ while the true phase is close to 0. Just due to this phase error, the initial decrease behavior is caused as shown in Fig. 16. With time proceeding to 0.01 s, the phase error decreases to a value less than $\pi/2$ seen in Fig. 17. As this small phase error, the response starts to keep a constant value near 0 or a waved tendency around 0. In fact, the phase error remains less than $\pi/2$ even after 0.01 s when the controlled response amplitude decrease to a convergence value.

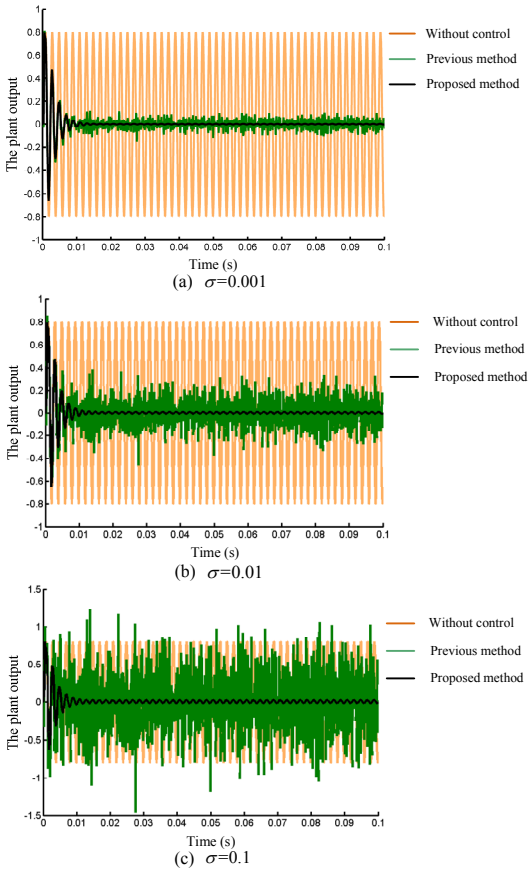

Fig. 16. Active control results with different variance.

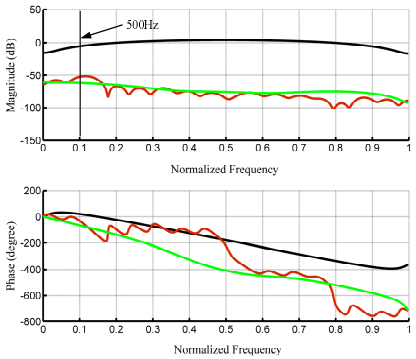

Fig. 17. Identification performance of secondary path.

5. Numerical simulations

On the basis of Sec. 2, actuators are placed onto the gear shaft with considering the symmetry of controlling and the diagrammatic sketch of a gear transmission with controlled system is shown in Fig. 18.

In Fig. 18, there are four acceleration sensors in simulation studies. The two sensors (numbers 1 and 2) are used to provide the reference signal for the algorithm, and the other two (numbers 3 and 4) will pick up error signals that are required also by the algorithm. To verify the ability of the proposed approach, the application to a gearbox is performed. To ensure

Table 4. Relative simulation parameters.

Parameters	Symbols	Numerical values
Gear mesh error	e	0
Bending stiffness of shaft (N/m)	$k_{bi}\,(i=1,2)$	4000
Mean mesh stiffness (N/m)	k	1000
Equivalent stiffness of roller bearing (10^6 N/m)	$k_i\,(i=1,2,3,4)$	7.1
Equivalent stiffness of ball bearing (10^6 N/m)	$k_j\,(j=1,2,3,4)$	5.3

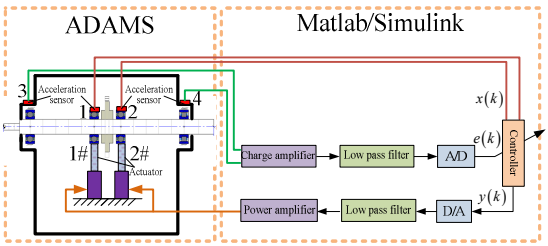

Fig. 18. Diagrammatic sketch with controlled system.

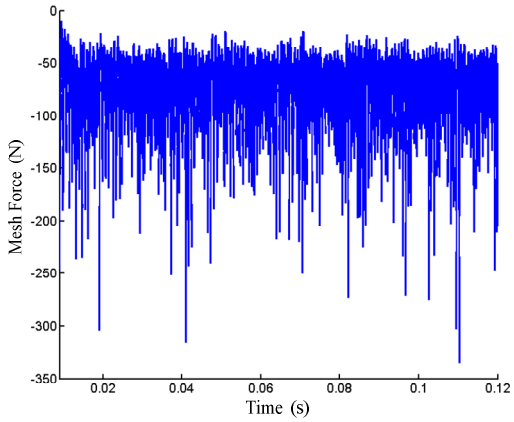

Fig. 19. Mesh force with respect to time.

a realistic assessment as possible, a united simulation technique is utilized by well-known softwares, ADAMS and Matlab/Simulink. In this simulation, the gearbox model is constructed in ADAMS software, in which the gear housing and the shafts are treated as flexible bodies based on Component mode synthesis (CMS) technique. The proposed adaptive filtering algorithm with online identification is performed in Matlab/Simulink by using the user-defined level-2 S function.

To verify the effectiveness of the proposed approach above, such references as bearing supports and gear housing surface should be selected as the position of evaluating the proposed active control algorithm. In addition, the previous method is also applied in our gearbox system, which is compared with the modified algorithm proposed in this paper. In simulation, we let the rotating speed $n=500$ r / min and the load torque $T_l=5$ N·m . Other relative simulation parameters are given in Table 4. In simulations, we assumed that orthogonal stiffness of each bearing is identical. Fig. 19 shows the mesh force with

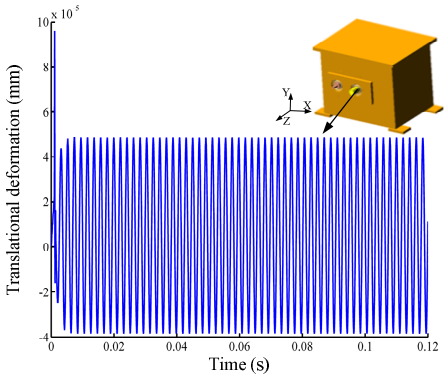

(a) Translational deformation in time domain

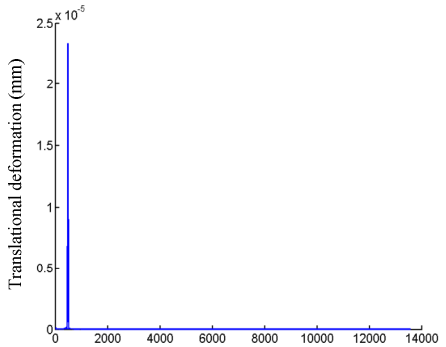

(b) Translational deformation in frequency domain

Fig. 20. The translational deformation of roller bearing inner ring center.

respect to varying-time along the line-of-action with considering gear backlash, from which we can see that the mesh force is unstable in the period of per revolution for gear pair due to gear backlash.

Under the condition without applying vibration control to the gearbox system, the translational deformation of bearing inner ring center along Y direction is shown in Figs. 20 and 21 and the translational deformation of bearing support location along Y direction is shown in Figs. 22 and 23.

According to the gear teeth and rotating speed, we know that the fundamental mesh frequency is 233.3 Hz. From Figs. 20-23, in time domain, an impulse occurs at the beginning of time due to existence of the load torque when gearbox system starts. Subsequently, it changes stably in a similar sinusoidal form. In frequency domain, the translation deformation peaks are mainly at 476.8 Hz close to the second harmonic frequency caused by gear backlash. In addition, as shown in Figs. 20 and 21, the roller bearing has a better vibration-absorbing performance than the ball bearing.

To verify the validity of the proposed method, the results in frequency domain obtained by utilizing active control are shown in Fig. 24.

In Fig. 24, the black solid line represents the translational deformation with respect to frequency for bearing support location under no control. Red solid line means the translational deformation with respect to frequency for bearing sup-

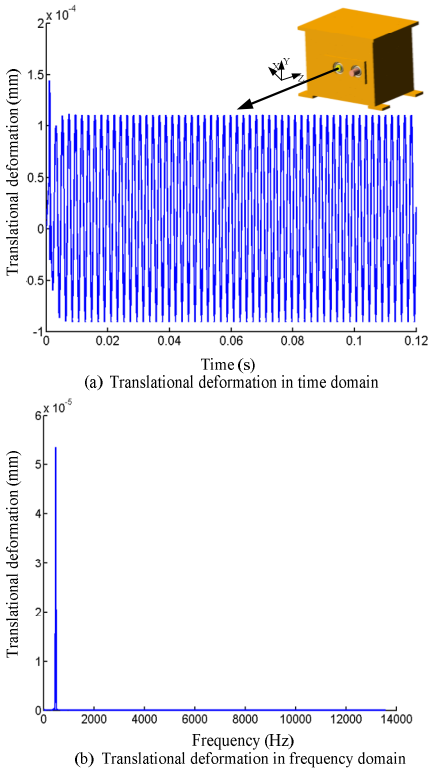

Fig. 21. The translational deformation of ball bearing inner ring center.

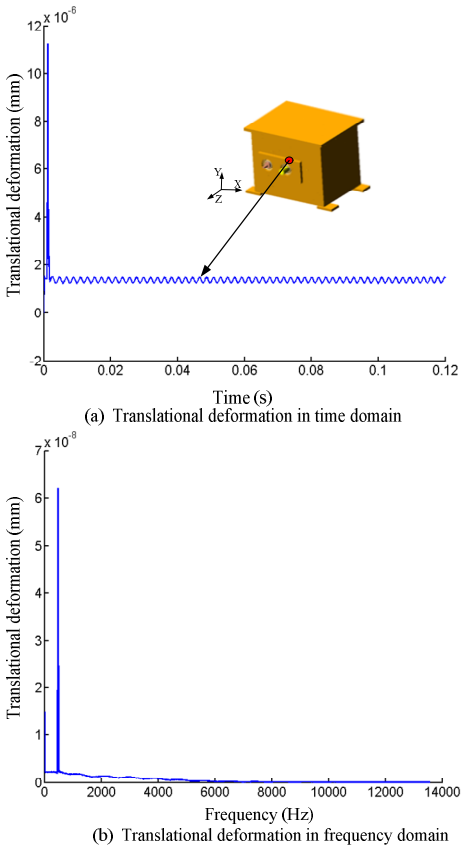

Fig. 22. The translational deformation of roller bearing support location.

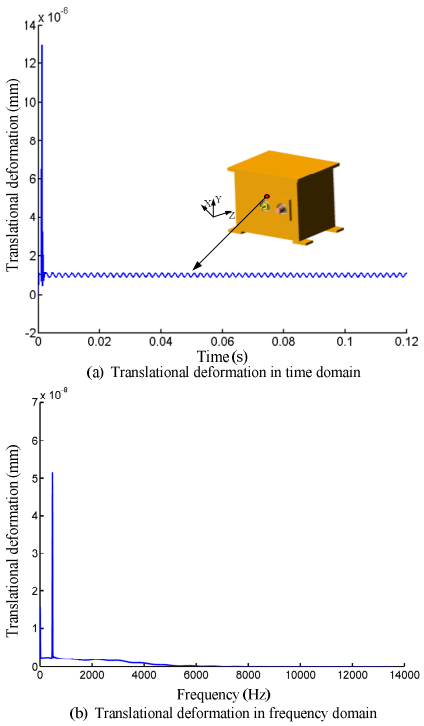

Fig. 23. The translational deformation of ball bearing support location.

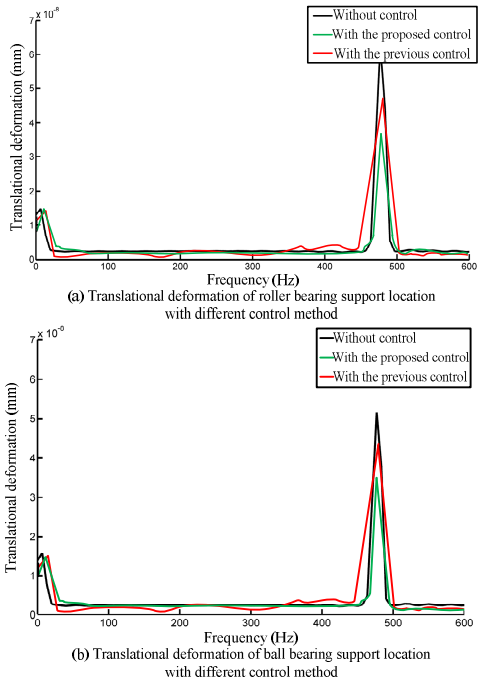

Fig. 24. Translational deformation of bearing support locations.

port location simulated by using Lim's method [4]. Green solid line denotes the translational deformation with respect to frequency for bearing support location simulated by employing the proposed method in this paper. Obviously, the peak value reduces to an extent at the second harmonic frequency when control strategy is implemented. Moreover, the pro-

posed method has more efficiency than the previous method.

6. Conclusions

As a guidance to future experimental work, a modified Fx-LMS algorithm with online secondary path identification was implemented to compute the effectiveness of applying that into an internal shaft transverse vibration control to suppress gear mesh vibration caused by gear backlash. The controller is designed by introducing another adaptive filter to track the primary path, and also a new identification input with error energy is incorporated in the process of secondary path identification, which improves the performance of the active vibration control system. The simulation results also demonstrate the efficiency of the proposed approach compared with the previous method, and further show the feasibility of applying the modified control strategy to gearbox vibration phenomena. According to the simulation results, we can draw several conclusions. First, the actuator location is configured well, and indirectly is shown from the united simulations. Second, the proposed algorithm with online secondary path identification is more robust than the previous method, in which the random noise has less influence on the whole system. Third, in applying this modified algorithm, the united simulation validates its efficiency. The last conclusion is that the modified control algorithm has been shown to work well using united simulation and to apply in a real gearbox system.

Acknowledgment

This work is supported by National Natural Science Fund (No. 11272026).

References

[1] E. Mucchi and A. Vecchio, Acoustical signature analysis of a helicopter cabin in steady-state and run up operational conditions, *Measurement*, 43 (2010) 283-293.

[2] T. A. Millott et al., Flight test of active gear-mesh noise control on the S-76 aircraft, *Proceedings of the 54th Annual Forum of the American Helicopter Society*, Washington, D.C. (1998).

[3] M. F. Li, T. C. Lim and W. S. Jr. Shepard, Modeling active control of a geared rotor system, *Smart Materials and Structures*, 13 (2004) 449-458.

[4] M. F. Li et al., Actuator design and experimental validation for active gearbox vibration control, *Smart Materials and Structures*, 15 (2006) 1-6.

[5] N. Sawalhi and R. B. Randall, Gear parameter identification in a wind turbine gearbox using vibration signals, *Mechanical Systems and Signal Processing*, 42 (2014) 368-376.

[6] G. T. Montague et al., Feed-Forward control of gear mesh vibration using piezoelectric actuators, *NASA Technique Memorandum-106366* (1994).

[7] B. Rebbechi, C. Howard and C. Hansen, Active control of gearbox vibration, *Proceeding of the Active Control of Sound and Vibration Conference*, Fort Lauderdale (1999) 295-304.

[8] M. H. Chen and M. J. Brennan, Active control of gear vibration using specially configured sensors and actuators, *Smart Materials and Structures*, 9 (2000) 342-350.

[9] Y. H. Guan, T. C. Lim and W. S. Jr. Shepard, Active vibration control of a gear pair using a direct adaptive control method, *Proc. SPIE 9th Int. Symp. On Smart Structures and Materials-Modeling, Signal Processing, and Control*, San Diego, 4693 (2002) 360-371.

[10] Y. H. Guan, T. C. Lim and W. S. Jr. Shepard, Direct hybrid adaptive control of gear pair vibration, *ASME J. of Dynamic Systems Measurement and Control*, 125 (2003) 585-594.

[11] Y. H. Guan, T. C. Lim and W. S. Jr. Shepard, Comparative analysis of actuator concept for active gear pair vibration control, *J. of Sound and Vibration*, 269 (2004) 273-294.

[12] Y. H. Guan, T. C. Lim and W. S. Jr. Shepard, Experimental study on active vibratiaa3on control of a gearbox system, *J. of Sound and Vibration*, 282 (2005) 713-733.

[13] R. G. Parker et al., Vibration propagation of gear dynamics in a gear-bearing-housing system using mathematical modeling and finite element analysis, *NASA/CR* (2012).

[14] S. A. Hambric et al., Rotorcraft transmission noise path model, including distributed fluid film bearing impedance modeling, *NASA Technical Report* (2010).

[15] F. B. Oswald et al., Effect of operating conditions on gearbox noise, *NASA Technical Memorandum-105331* (1992).

[16] F. B. Oswald et al., Influence of gear design parameters on gearbox radiated noise, *NASA Technical Memorandum-106511* (1994).

[17] W. J. Gao, L. Wang and Y. G. Liu, Analysis on vibration transmission characteristics of box-like power structure, *J. of Beijing University of Aeronautics and Astronautics* (2015) [in press].

[18] W. J. Gao and L. Wang, Research on dynamic transmission characteristics of box-like structures based on a hybrid model method, *IEEE/ASME International Conference on Advanced Intelligent Mechatronics*, Busan, South Korea (2015) 7-11 [in press].

[19] L. J. Eriksson, Use of rand noise for online transducer estimate in an adaptive attenuation system, *Acoust. Soc. Amer.*, 85 (1989) 797.

[20] X. Y. Zhang and C. J. Yi, Neural network method for online secondary path identification, *Noise and Vibration Control*, 1 (2009) 69-72 [in Chinese].

[21] I. T. Ardekani and W. H. Abdulla, Theoretical convergence analysis of Fx-LMS algorithm, *Signal Processing*, 90 (12) (2010) 3046-3055.

[22] S. M. Kuo and D. R. Morgan, Active noise control: a tutorial review, *Proc. IEEE*, 87 (1999) 943-973.

[23] S. M. Kuo, M. Tahernezhaadi and W. Hao, Convergence analysis of narrowband active noise control system, *IEEE Trans. Circuits Syst. II*, 46 (1999) 220-223.

Weijin Gao received the Ph.D. in Mechatronics Engineering from Beihang University. His research interests include dynamic topology optimization and active vibration control.

Liang Wang received the B.E., M.E. and Ph.D. in Mechanical Engineering from the Harbin Shipbuilding Engineering Institute in 1985, Harbin Institute of Technology in 1988, and Beihang University in 2000. Since 2005, he has been a Professor with School of Automation Science and Electrical Engineering, and the Director of Engineering Training Center. His research interests include mechatronics, vibration control, and human-machine system.